



www.sciencemag.org/cgi/content/full/1129185/DC1

Supporting Online Material for

A Long-Period, Violently Variable X-ray Source in a Young Supernova Remnant

A. De Luca,* P. A. Caraveo, S. Mereghetti, A. Tiengo, G. F. Bignami

*To whom correspondence should be addressed. E-mail: deluca@iasf-milano.inaf.it

Published 6 July 2006 on *Science Express*
DOI: 10.1126/science.1129185

This PDF file includes:

SOM Text
Figs. S1 to S5
Table S1
References

Supporting online material

1.XMM-Newton/EPIC data analysis

Observations and data reduction. The long 2005 XMM-Newton observation of 1E started on August 23rd 2005 and lasted for 89.2 ks. The EPIC/pn was operated in Small Window mode with the thin optical filter; the EPIC/MOS1 and MOS2 were operated in Full Frame mode with the medium optical filter. Raw data were processed with the most recent release of the XMM-Newton Science Analysis Software (SASv6.5.0) using standard pipelines. Dead-time corrected exposure times were of 86.1 ks, 86.2 ks and 61.2 ks in the MOS1, MOS2 and pn detector, respectively. No time filtering to screen high particle background episodes was applied. Standard event PATTERN filtering was used (PATTERN 0-4 and 0-12 for the pn and MOS, respectively). Owing to the bright and patchy emission from the surrounding SNR, selection of source and background events required a particular care. We extracted background counts from a 20'' radius circle centered at RA 16:17:42.4, Dec -51:02:38, where the surface brightness is comparable to the one seen in the source region (as estimated using high-resolution Chandra images). Selecting source events from a 15'' radius circle yields background-subtracted count rates of 0.382 ± 0.003 cts s⁻¹, 0.132 ± 0.001 cts s⁻¹, 0.139 ± 0.001 cts s⁻¹ in the 0.5-8 keV energy range for the pn, MOS1 and MOS2 in 2005. The same event selection was used to extract both light curves and spectra. Different choices of background regions result in somewhat different best fit values for the spectral parameters (mainly the N_H), but do not affect the source variability analysis.

Time-integrated spectroscopy. Time-integrated spectra for source and background were extracted for each EPIC instrument from the regions described above. Source spectra were rebinned in order to have at least 30 counts per spectral bin. Ad-hoc response matrices and effective area files were generated using SAS tasks `rmfgen` and `arfgn`. Spectral analysis was performed with the XSPEC v11.3 software, fitting simultaneously pn and MOS spectra in the

0.5-8 keV energy range. Single component models (including interstellar absorption) did not yield satisfactory results: while a power law is clearly inadequate (reduced $\chi^2 > 2.2$, 492 d.o.f.), a blackbody or a thermal bremsstrahlung curve yield somewhat better fits (reduced χ^2 of 1.43 and 1.37, respectively, 492 d.o.f.), although inspection of the residuals shows significant, structured deviations. Better results were obtained using double component models consisting of a dominant blackbody curve complemented with a second blackbody (reduced $\chi^2=1.18$, 490 d.o.f.) or with a power law (reduced $\chi^2=1.19$, 490 d.o.f.). The best fit parameters are reported in table S1. The observed spectra together with the best fit double blackbody model are shown in Fig.S1, where residuals are also plotted in the lower panel.

Timing analysis. Source and background light curves were extracted for each instrument using the regions described above. The source periodicity was immediately apparent. Since the light curve is sharply peaked, it cannot be satisfactorily fitted using a sin function. Indeed, while a sin function fit to the combined (pn+MOS) background-subtracted light curve (0.5-8 keV) yields a reduced $\chi^2=2.67$ (84 d.o.f.), adding a second harmonic improves the overall fit quality (reduced $\chi^2=1.63$, 82 d.o.f.). However, the resulting best fit period of $P=6.67\pm 0.03$ hr remains identical. MOS and pn light curves were also independently analysed, yielding fully consistent results. The Pulsed Fraction, defined as $PF=(CR_{\max}-CR_{\min})/(CR_{\max}+CR_{\min})$, where CR_{\max} and CR_{\min} are the observed background-subtracted count rates at the peak and at the minimum, is very large: in the 0.5-8 keV range the PF turns out to be $43.5\pm 1.8\%$. Although the pulse profile does not change significantly as a function of energy (Fig.S2), there are hints for substructures in the soft band (0.5-2 keV) but not in the hard one (2-8 keV). The pulsed fraction increases significantly as a function of energy, going from $37.1\pm 2.8\%$ in the soft band to $56.8\pm 2.9\%$ in the hard band. The corresponding hardness ratio (Fig.S1), defined as $HR=(CR_{\text{Hard}}-CR_{\text{Soft}})/(CR_{\text{Hard}}+CR_{\text{Soft}})$, where CR_{Hard} and CR_{Soft} are the background-subtracted count rates in the 2-8 keV and in the 0.5-2 keV ranges, shows that the source emission is

markedly harder at the peak and softer at minimum, hinting a significant spectral evolution as a function of the 6.67 hr cycle. A search for fast periodicity was also performed, using standard fast Fourier transform techniques. Since our high resolution timing data have a ~ 6 ms sampling, we searched for periodicities larger than 12 ms. No pulsed signal was found. Assuming a sinusoidal pulse shape, we constrain the source pulsed fraction to be $< 10\%$ (99% confidence level).

Phase-resolved spectroscopy. In order to study the spectral evolution as a function of the 6.67 hr cycle, we extracted source and background spectra selecting only events within the phase intervals corresponding to the peak and to the minimum of the light curve (Fig.S2 A). The spectral analysis was performed assuming the double blackbody model best fitting the time-integrated spectrum. As a first step, we kept all parameters fixed to their best fit values for the time-integrated spectrum, allowing only the overall normalization factor to vary. This approach yielded unacceptable fits to the data (reduced $\chi^2=3.75$, 632 d.o.f.), with residuals clearly showing the source spectrum to be softer at minimum and harder at the peak. A better fit was obtained allowing the normalizations of the two spectral components to vary independently (reduced $\chi^2 \sim 1.4$, 628 d.o.f.); a further improvement (reduced $\chi^2=1.15$, 624 d.o.f.) was achieved allowing the blackbody temperatures to vary. Such best fit parameters are reported in the caption to Fig.S2. The spectra obtained for the peak and the minimum are shown in the upper panel of Fig.S2 (B), while the lower panel gives the ratio between the peak spectrum and the best fit model for the spectrum of the minimum (renormalized to the same number of counts). The spectral hardening at the peak is apparent.

The September 2001 observations.

Observations and data reduction. The September 2001 dataset results from the merging of two observations. The first pointing (30 ks) was aimed at the energetic pulsar PSR J1617-5055 (located ~ 7.5 arcmin North of RCW103) and useful data on 1E (imaged at 7.5 arcmin

offaxis) were collected only by the MOS cameras (operated in Full Frame mode with the medium optical filter). The satellite then slewed to RCW103 and collected 20 ks of data on 1E using all EPIC cameras, operated with a setup identical to that used in 2005. Data reduction and analysis was performed as for the 2005 observation. Dead-time corrected exposure time was of 27.8 ks (off-axis observation) + 18.8 ks (on-axis observation) and 27.8+18.9 ks for MOS1 and MOS2 and 12.9 ks for the pn. The background-subtracted on-axis count rate of 1E was of $1.936 \pm 0.013 \text{ cts s}^{-1}$, $0.692 \pm 0.006 \text{ cts s}^{-1}$ and $0.701 \pm 0.006 \text{ cts s}^{-1}$ for the pn, MOS1 and MOS2, respectively, i.e. a factor ~ 5 higher than in 2005.

Time-integrated spectroscopy. The spectral analysis was performed following the procedure described for the 2005 observation. Two component models, either encompassing two blackbody curves (reduced $\chi^2=1.09$, 517 d.o.f.), or the combination of a blackbody curve and a power law (reduced $\chi^2=1.14$, 517 d.o.f.) yielded the best fit to the data, as reported in Table S1. The time-averaged observed flux is $9.9 \times 10^{-12} \text{ erg cm}^{-2} \text{ s}^{-1}$ (0.5-8 keV), i.e. ~ 6 times higher than in 2005. As shown in Fig.S3, the spectrum of the source in its 2001 “high state” is remarkably harder than in the “low state” of 2005. To reproduce the 2001-2005 spectral change, both spectral components in both models have to vary.

Timing analysis. Background-subtracted light curves were produced following the procedure described for the 2005 observation. In order to combine the data collected in the two (off-axis and on-axis) observations to produce a unique, 50 ks long light curve, we computed count-rate to flux conversion factors accounting for the observed source spectrum (see above) as well as for the significant vignetting affecting the first section of the data. The resulting light curve (0.5-8 keV energy range) is shown in Fig.2. With a light curve covering ~ 2 periods, the source periodicity may be clearly recognized, in spite of the 3 ks interruption. The pulse profile is very complex, with a narrow dip, ~ 2500 s long, occurring after the highest peak and a secondary, less pronounced, dip, separated by 0.5 in phase from the first one. The central

times of such dips (computed by fitting a gaussian curve to their profile) were used to evaluate the period, which turned out to be of 6.72 ± 0.08 hr, consistent with the value measured in 2005. The pulsed fraction is $PF = 11.7 \pm 1.4\%$, remarkably lower than in 2005. We note that, in absolute units, the pulsed flux is very similar to the value observed in 2005, i.e. $\sim 2 \times 10^{-12}$ erg cm⁻² s⁻¹.

Time-resolved spectroscopy. In order to investigate the spectral variation along the periodic cycle, we extracted time-resolved spectra selecting two 2500 s time intervals centered on the lowest dip and on to the highest peak, respectively. The time-integrated double blackbody best fit model was assumed as a template. A simple renormalization of such model does not fit well the data, since the dip spectrum is markedly harder. The spectral evolution may be described (reduced $\chi^2 = 1.02$, 348 d.o.f.) by a smaller emitting radius of the dominant blackbody, possibly coupled to extra absorption along the line of sight, during the dip. However, a detailed modelling is hampered by the limited statistics.

2. Chandra/Advanced CCD Imaging Spectrometer (ACIS) data analysis.

“Level 1” event files were retrieved from the public Chandra archive and processed with standard pipelines (`acis_process_events`, *SI*) using the Chandra Interactive Analysis of Observations (CIAO v3.2.1) software package. Source events were selected from circular regions corresponding to encircled energy fractions of ~ 0.9 . In February 2000 the source was in a very high state with the data heavily affected by pile-up. To overcome the problem, we excluded the PSF core, extracting source events from an annulus with inner and outer radii of 2.5” and 6”, respectively, and we recomputed the total flux evaluating the encircled energy fraction in the annular region (a conservative 20% error on the flux was assumed in such case). Background events were selected in all cases from 20” radius regions located close to the target. We extracted spectra for source and background and we generated appropriate response matrices and effective area files using the `psextract` (*SI*) script. Source spectra were

rebinned in order to have at least 30 counts per channel. Each spectrum was fitted in XSPEC v11.3 in the 0.8-8 keV energy range using a double blackbody curve modified by interstellar absorption. The observed flux in the 0.5-2 keV range was then computed for each epoch using the corresponding best fit model.

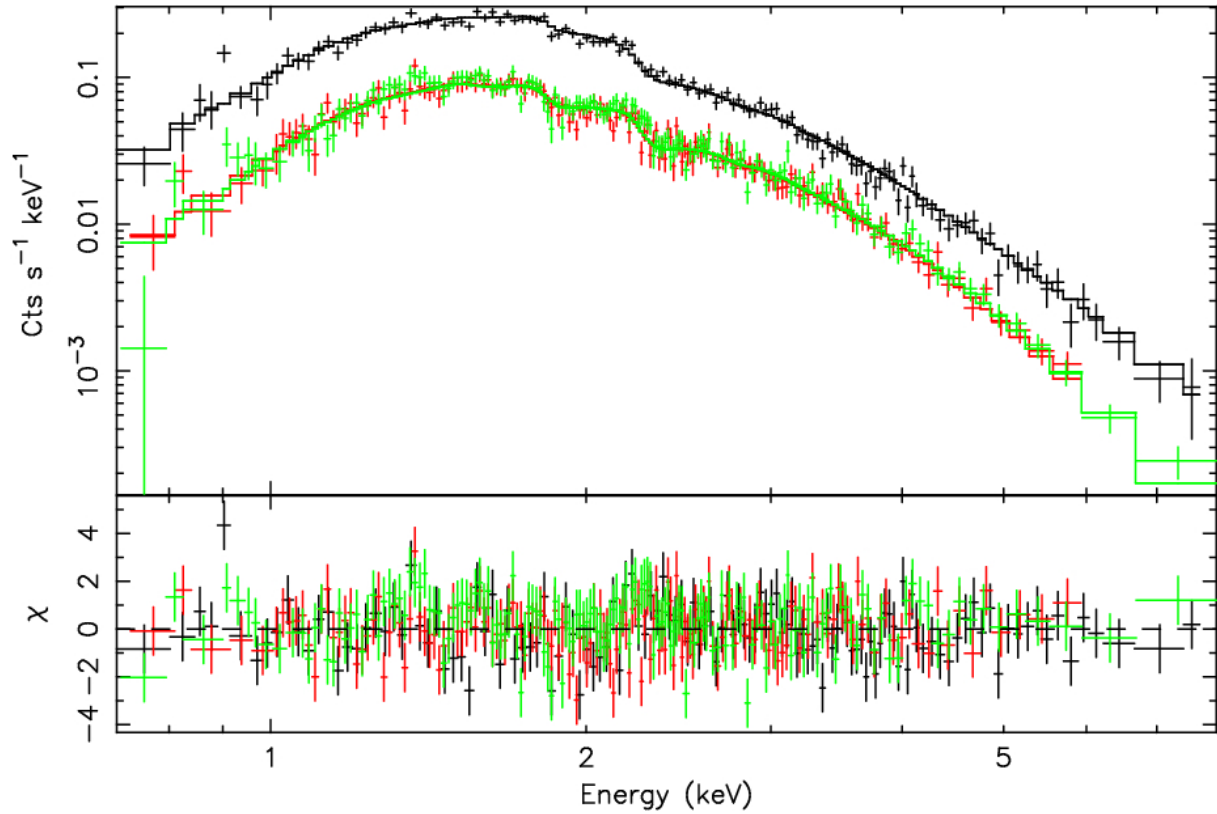


Figure S1. August 2005 spectrum of 1E as observed by the three EPIC cameras. The upper panel shows the time-integrated spectrum of 1E as observed with EPIC. Black, green and red data points are from the pn, MOS1 and MOS2 cameras, respectively. The best fit model, consisting of the sum of two blackbody curves (see text), is overplotted. The lower panel shows the residuals in units of statistical errors.

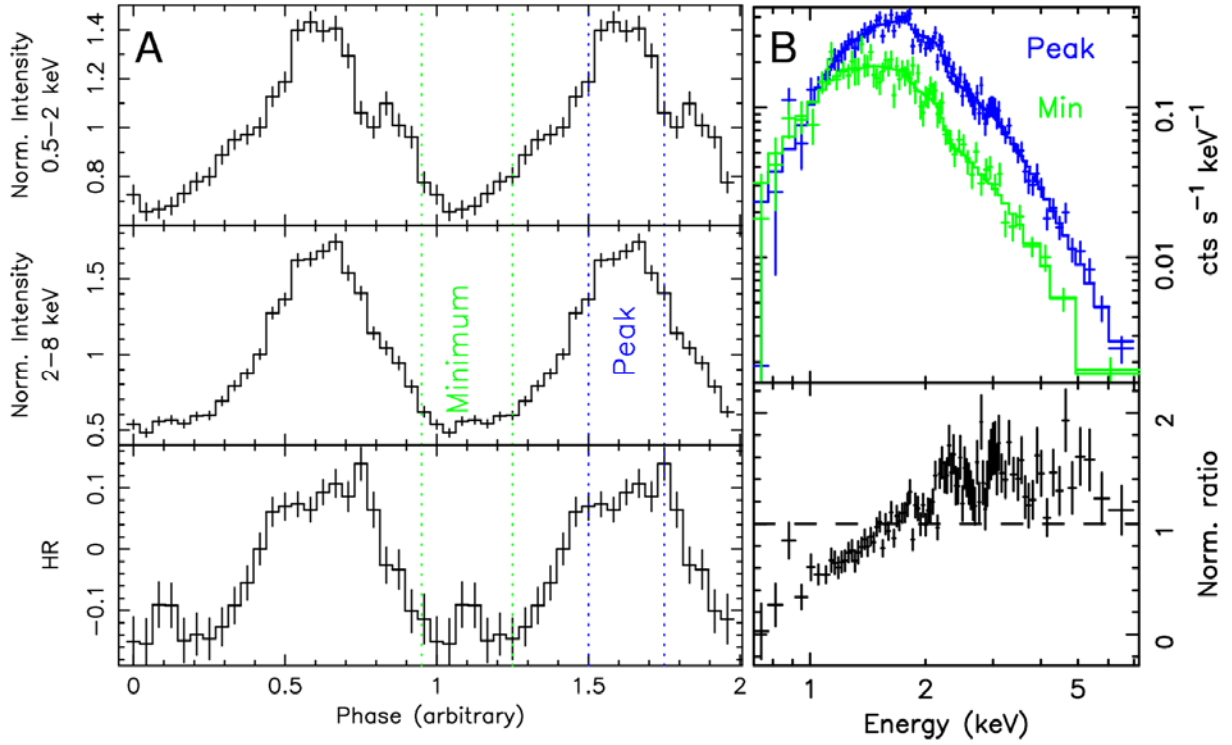


Figure S2. Spectral evolution of 1E over its 6.67 hours periodicity, as observed in August 2005. **(A)** Folded light curves (normalized to the average flux value) in the soft (0.5-2 keV) and in the hard (2-8 keV) ranges and corresponding hardness ratio, defined as $HR = (Cts_{2-8} - Cts_{0.5-2}) / (Cts_{2-8} + Cts_{0.5-2})$. Note the spectral hardening during the pulse peak, as well as the energy dependence of the pulsed fraction (PF=37.1±2.8% in the soft band, PF=56.8±2.9% in the hard band). **(B)** Spectra of 1E as extracted from the phase intervals corresponding to the peak (blue) and to the minimum (green), as well as the ratio between the peak spectrum and the renormalized best fit model for the minimum. The spectral evolution is quite complex: assuming as a template the double blackbody model, we obtain at minimum $N_H = 5 \pm 1 \times 10^{21} \text{ cm}^{-2}$; temperature and emitting radius of the dominant blackbody $kT_{bb1} = 0.47 \pm 0.03$ and $R_{bb1} = 560 \pm 60 \text{ m}$; temperature and emitting radius of the second blackbody $kT_{bb2} = 1.4 \pm 0.7 \text{ keV}$, $R_{bb2} < 80 \text{ m}$; at the peak $N_H = 9 \pm 1 \times 10^{21} \text{ cm}^{-2}$, $kT_{bb1} = 0.54 \pm 0.02$, $R_{bb1} = 750 \pm 40 \text{ m}$, $kT_{bb2} = 1.3 \pm 0.4 \text{ keV}$, $R_{bb2} = 40 \pm 20 \text{ m}$ (errors are at 90% confidence level for a single parameter).

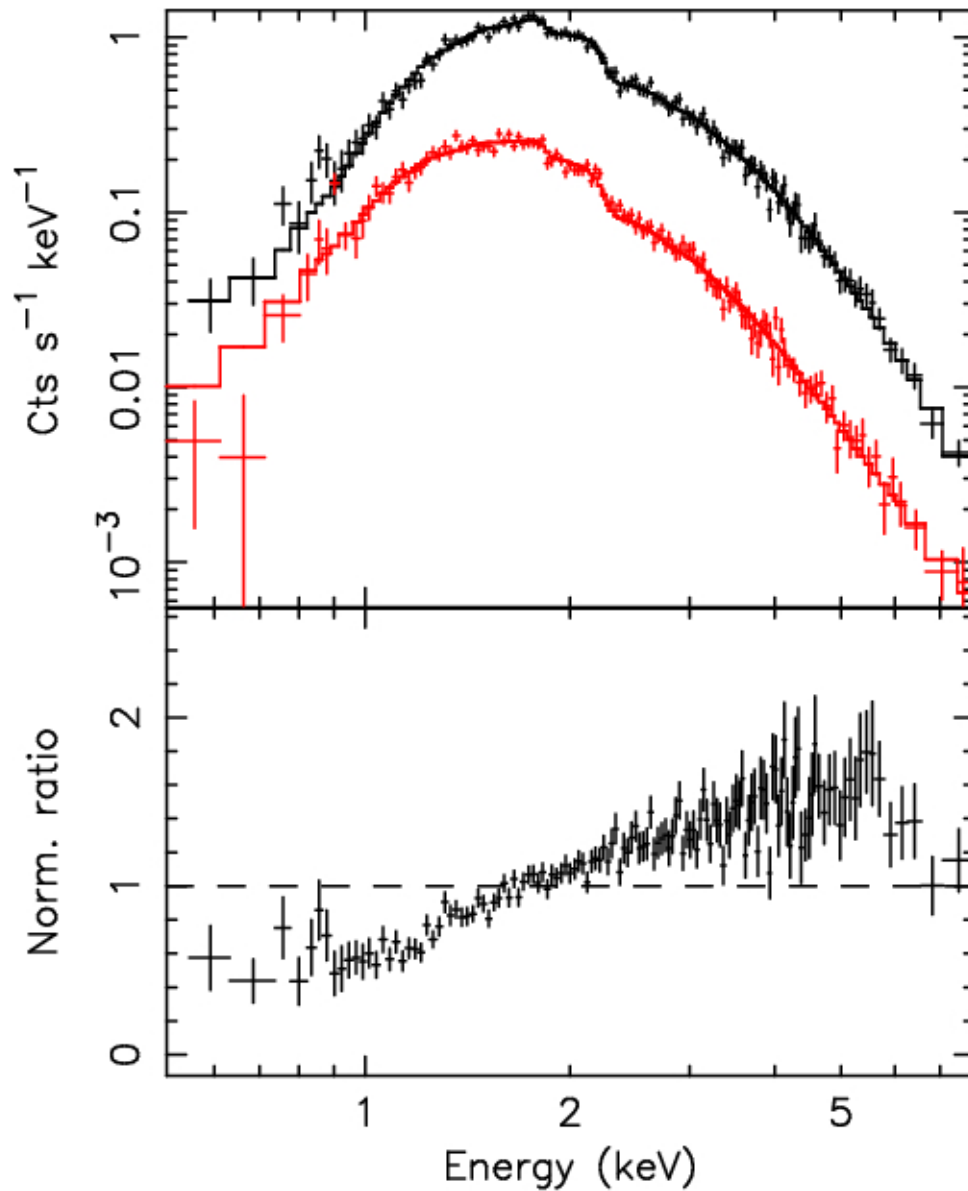


Figure S3. The upper panel shows the time-integrated pn spectrum of 1E in the high state of 2001 (black data points) together with the best fit double blackbody model (black line); the 2005 pn spectrum (red data point) and best fit model (red line) are also plotted. The lower panel shows the ratio between the 2001 spectrum and the 2005 best fit model (renormalized to the 2001 number of counts). The 2001 spectrum is clearly harder than the 2005 one.

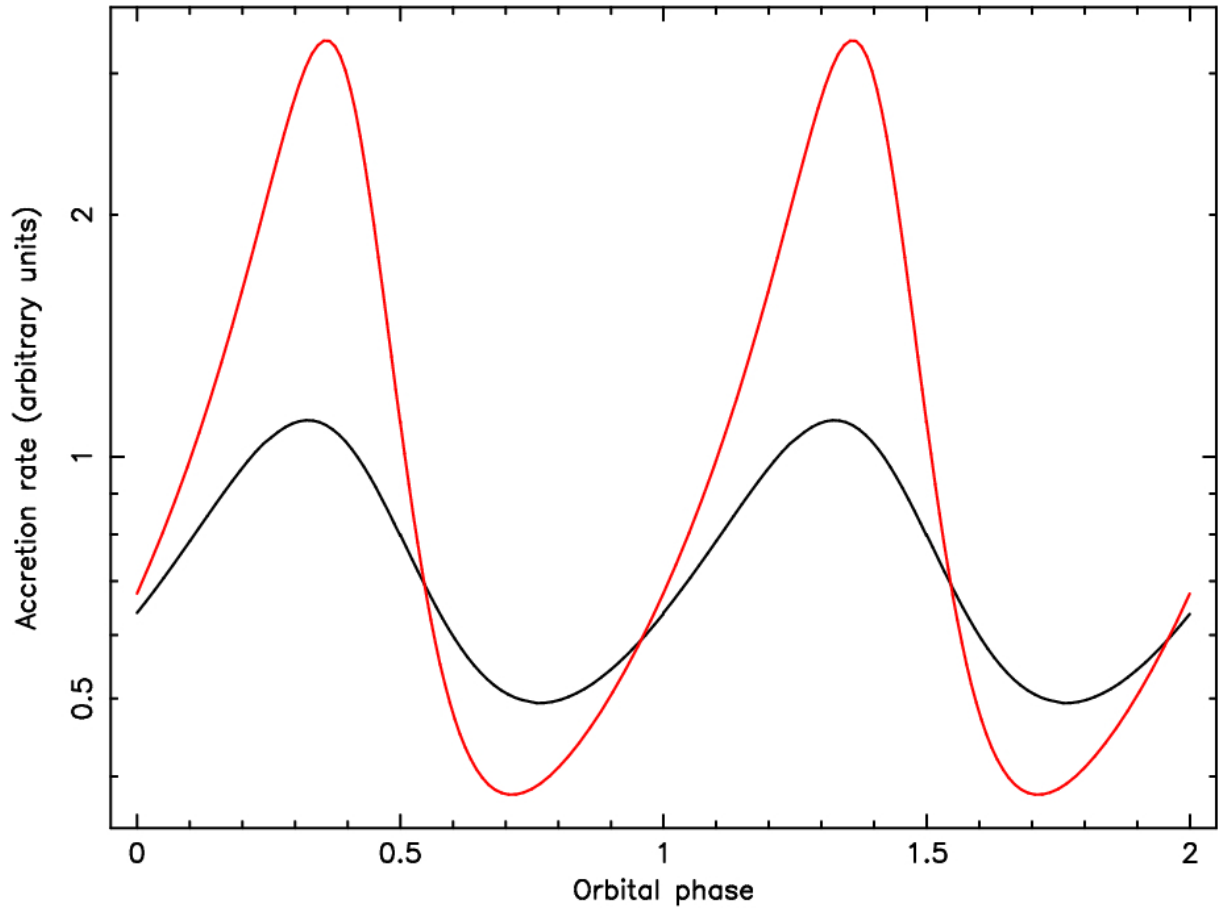


Figure S4. Expected modulation of the mass fraction f of the companion star wind captured by the accreting object in an eccentric system. We followed the Bondi-Hoyle approach, assuming a $1.4 M_{\odot}$ neutron star and a 6.67 hr orbital period. The black line corresponds to the case of a $0.4 M_{\odot}$ companion star and an eccentricity of 0.2; the red line corresponds to the case of a $0.2 M_{\odot}$ companion star and an eccentricity of 0.5. A companion wind velocity of 300 km s^{-1} was assumed. Phase 0 correspond to the periastron. A remarkable modulation is obtained in both cases, with a single peak in the descending part of the orbit. The resulting shape is very similar to the observed light curve of 1E in its low state.

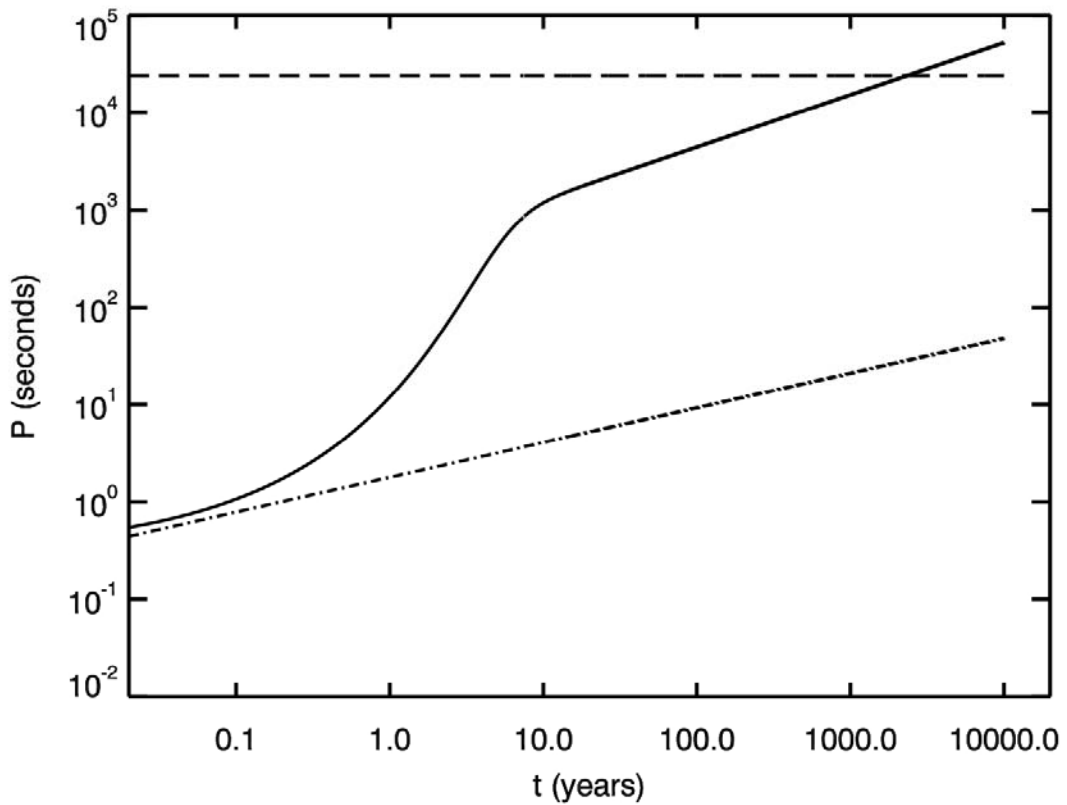


Figure S5. Spin-down history of 1E, resulting from propeller interaction with the material of a SN debris disc. The source spin period as a function of time is plotted as a black solid line. The dot-dashed line shows the faster spin period at which propeller interaction may occur. For faster rotation rates the pressure of the rotating dipole would exceed the pressure of the infalling material, pushing the disc outside the light cylinder (ejector phase), preventing the propeller effect. Following (24, 25), assuming a magnetic field of 5×10^{15} G, a disc mass of $3 \times 10^{-5} M_{\odot}$ and a birth period of 0.3 s, an early ejector phase is avoided and the NS starts spinning down in the propeller regime. In ~ 2 kyr the NS rotation is quenched to $P \sim 6.67$ hr (~ 24 ks), marked by the horizontal dashed line.

Table S1. Results of XMM-Newton/EPIC time-integrated spectroscopy.

Year	2005	2005	2001	2001
Model	BB+BB	BB+PL	BB+BB	BB+PL
N_{H} (10^{22} cm $^{-2}$)	0.65±0.04	0.85±0.20	1.08±0.05	1.35±0.15
kT_{bb1} (keV)	0.51±0.01	0.52±0.01	0.50±0.02	0.54±0.01
R_{bb1} (m)	610±35	570±30	1560±120	1310±50
kT_{bb2} (keV)	1.0 $^{+0.4}_{-0.2}$	-	0.93 $^{+0.13}_{-0.09}$	-
R_{bb2} (m)	35 $^{+22}_{-12}$	-	220 $^{+100}_{-60}$	-
Γ	-	2.9 $^{+0.4}_{-0.9}$	-	3.0 $^{+0.3}_{-0.5}$
$F_{\text{obs}}^{\text{a}}$ (erg cm $^{-2}$ s $^{-1}$)	1.7×10^{-12}	1.7×10^{-12}	9.9×10^{-12}	9.9×10^{-12}
$L_{\text{bb1}}^{\text{b}}$ (erg s $^{-1}$)	3.0×10^{33}	2.9×10^{33}	2.0×10^{34}	1.9×10^{34}
$L_{\text{bb2}}^{\text{c}}$ (erg s $^{-1}$)	3.8×10^{32}	-	4.6×10^{33}	-
L_{PL}^{d} (erg s $^{-1}$)	-	1.6×10^{33}	-	1.7×10^{34}
χ^2_{v}	1.18	1.19	1.09	1.14
d.o.f.	490	490	517	517

^a Observed Flux, 0.5-8 keV

^b Bolometric luminosity of dominant blackbody

^c Bolometric luminosity of second blackbody

^d Luminosity of the power law component, 0.5-8 keV

References and notes.

S1. See <http://cxc.harvard.edu/ciao/threads/all.html>